Peripheral re-localization of constitutive heterochromatin advances its replication timing and impairs maintenance of silencing marks

Kathrin S. Heinz[1], Corella S. Casas-Delucchi[1], Timea Török[1], Dusan Cmarko[2], Alexander Rapp[1], Ivan Raska[2] and M. Cristina Cardoso[1,*]

[1]Cell Biology and Epigenetics, Department of Biology, Technische Universität Darmstadt, 64287 Darmstadt, Germany and [2]Institute of Biology and Medical Genetics, First Faculty of Medicine, Charles University and General University Hospital in Prague, 128 00 Prague, Czech Republic

ABSTRACT

The replication of the genome is a highly organized process, both spatially and temporally. Although a lot is known on the composition of the basic replication machinery, how its activity is regulated is mostly unknown. Several chromatin properties have been proposed as regulators, but a potential role of the nuclear DNA position remains unclear. We made use of the prominent structure and well-defined heterochromatic landscape of mouse pericentric chromosome domains as a well-studied example of late replicating constitutive heterochromatin. We established a method to manipulate its nuclear position and evaluated the effect on replication timing, DNA compaction and epigenetic composition. Using time-lapse microscopy, we observed that constitutive heterochromatin, known to replicate during late S-phase, was replicated in mid S-phase when repositioned to the nuclear periphery. Out-of-schedule replication resulted in deficient post-replicative maintenance of chromatin modifications, namely silencing marks. We propose that repositioned constitutive heterochromatin was activated in *trans* according to the domino model of origin firing by nearby (mid S) firing origins. In summary, our data provide, on the one hand, a novel approach to manipulate nuclear DNA position and, on the other hand, establish nuclear DNA position as a novel mechanism regulating DNA replication timing and epigenetic maintenance.

INTRODUCTION

The duplication of the genome is a highly complex process organized in a spatial and temporal manner (reviewed in (1)). On a cytological level, DNA replication is detectable as discrete sub-nuclear foci, where each focus corresponds to a cluster of coordinately activated replication forks (2–5), which can be resolved using superresolution light microscopy (6–8). During S-phase progression, the spatial distribution of these foci changes 'following' chromatin condensation level and leading to distinct nuclear patterns associated with early (euchromatin), mid (facultative heterochromatin) and late replicating (constitutive heterochromatin) chromosomal regions (Figure 1). This spatio-temporal organization of DNA replication is intrinsically related to the coordination of origin firing at distinct chromatin and nuclear regions, reflecting the higher order packing of the genome (reviewed in (9–11)). The plasticity of DNA replication timing is not sequence driven, as up until now no consensus origin sequence was identified in higher eukaryotes (12–15). Even in budding yeast, where replication origins are defined at the sequence levels, excising them from their endogenous locus can result in changes in their timing of firing during S-phase (16). On the other hand, DNA and histone modifications have been identified to play a central role in the definition of chromatin structure and replication progression (reviewed in (17)). Several lines of evidence support the idea that DNA replication timing is dictated by the chromatin structure as specific chromatin modifications correlate with DNA replication timing, such as histone acetylation with early replication in Drosophila (18) and H3K9 trimethylation (H3K9me3) or H4K20 trimethylation (H4K20me3), which are associated with late DNA replication (19–22). Moreover, disrupting chromatin modifications can lead to changes in DNA replication timing (19,23–26) indicating a possible interplay be-

*To whom correspondence should be addressed. Tel: +49 6151 16 21882; Fax: +49 6151 16 21880; Email: cardoso@bio.tu-darmstadt.de
Present address: Corella S. Casas-Delucchi, Chromosome Replication Laboratory, The Francis Crick Institute, London NW1 1AT, United Kingdom; Timea Török, Hämatologie/Onkologie, Medizinische Klinik II- Universitätsklinikum Frankfurt, 60595 Frankfurt am Main, Germany.
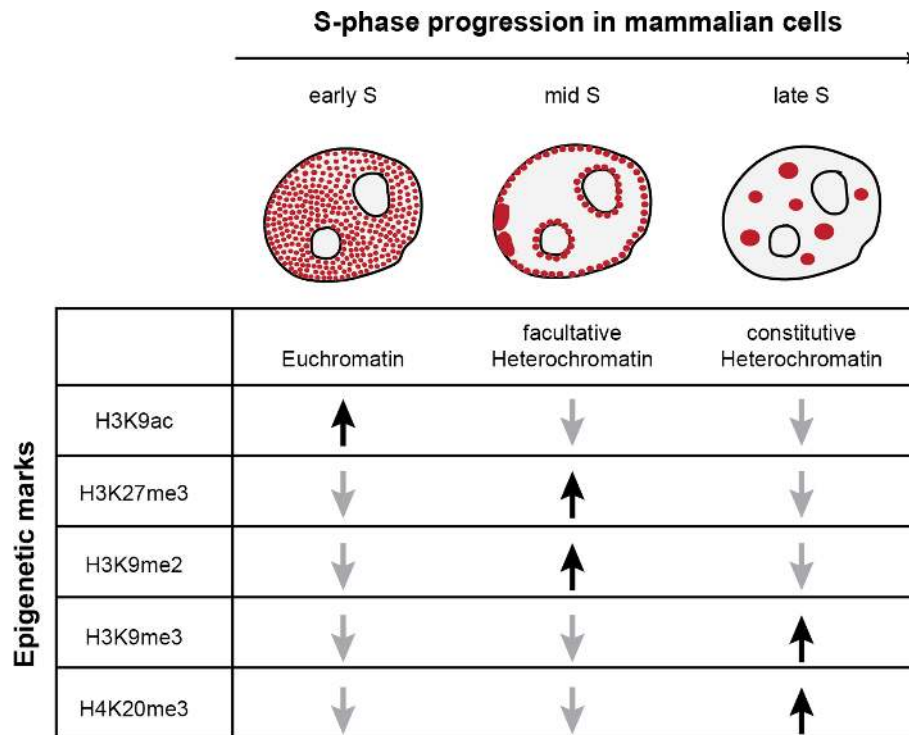
S-phase progression in mammalian cells

Figure 1. Summary of epigenetic modifications, chromatin types and DNA replication timing. Schematic images depict DNA replication foci patterns (red) during S-phase progression in mammalian cell nuclei. In early S-phase, when mostly euchromatin is replicated, a multitude of small replication foci are distributed throughout the whole nucleus. In mid S-phase, DNA replication foci are mostly concentrated at the nucle(ol)ar periphery and at the inactive X-chromosome(s). In this substage, mostly facultative heterochromatin is replicated. In late S-phase, replication foci mostly colocalize with constitutive heterochromatin (chromocenters) in mouse cells. Post-translational modifications of histones typical for the different chromatin types are indicated below. Less compacted euchromatin contains hyperacetylated histones. In contrast histones in heterochromatin are hypoacetylated and hypermethylated at the amino acid residues indicated. This is correlated with a more compacted structure and later DNA replication timing.

tween chromatin state and DNA replication timing. However, the mechanisms by which chromatin composition regulates the timing of origin firing and, vice-versa, how replication timing affects chromatin state, remain unclear. Circumstantial evidence correlates the spatial reorganization of chromatin at the end of mitosis / beginning of G1 phase of the cell cycle with the setup of the replication program (27). In budding yeast, an early firing origin was artificially tethered to the nuclear envelope (28) to study a regulatory effect of sub-nuclear position on its DNA replication timing. The peripheral positioning was not sufficient to delay the firing of this early origin. Hence, the available evidence does not provide an answer to whether nuclear architecture and positioning of chromatin, chromatin state and replication timing depend on each other.

Here, we set up a targeting strategy to investigate the effect of sub-nuclear localization of DNA within the mammalian nucleus on its replication timing and chromatin state. We made use of constitutive heterochromatin as it exhibits a distinct chromatin landscape characterized by high levels of DNA methylation, H3K9 trimethylation and histone hypoacetylation. In mice, these regions assemble into higher order aggregates known as chromocenters (29), composed of ∼10^5 major satellite DNA repeats that can be visualized by staining the DNA as round, highly condensed, prominent structures in the nucleus (30). We manipulated the nuclear localization of late replicating chromocenters by

juxtaposing them next to mid replicating facultative heterochromatin at the nuclear periphery to elucidate the impact of nuclear position of DNA on its replication timing and epigenetic composition. We were able to observe an advanced DNA replication timing of repositioned chromocenters accompanied by a decondensation of repositioned constitutive heterochromatin, as well as a progressive loss of silencing histone marks. We, therefore, conclude that the nuclear position plays a role in regulating DNA replication timing in mammalian cells.

MATERIALS AND METHODS

Expression plasmids

Expression vector encoding the complete rat Mecp2 ORF fused in frame to the NH_2 terminus of the enhanced GFP to construct the Mecp2-GFP (pc = plasmid collection number, pc1121) was described before (31) and was used here to detect methylated cytosines abundant at chromocenters. The second element of the targeting strategy was a GBP-Lamin B1 (pc1467), an expression vector encoding the sequence of the GFP-binding V_HH domain (32–34) fused to the human Lamin B1 coding sequence. As a control for the targeting assay the GFP-binding V_HH domain was removed by restriction with XhoI and SacII enzymes, followed by a treatment with Klenow polymerase large fragment to create blunt ends and re-ligation, to es-

tablish an expression vector with human Lamin B1 alone (pc2809). For sequence-specific chromocenter recognition by binding major satellite (ms) DNA, we performed double-transfections with GBP-Lamin B1 or Lamin B1 alone in combination with either msTALE (pc3086) (35), msPZF (pc1803) (36) or triple transfection with msCRISPR/dCas9 (pc3147, pc2942) (37) (Supplementary Figure S1).

Cell culture and transfection

C2C12 mouse myoblasts (38) were grown at $37°C$, $5\%\ CO_2$, in Dulbecco's modified Eagle's medium (DMEM) supplemented with 20% fetal calf serum and 1 μM gentamycin. Mouse embryonic fibroblasts (MEF) (39) were grown at $37°C$, $5\%\ CO_2$, in DMEM supplemented with 10% fetal calf serum and 1 μM gentamycin. Cell lines stably expressing mRFP-PCNA were kindly provided by the Leonhardt laboratory (LMU, Munich, Germany). These cell lines were established using an expression vector encoding a mRFP-tagged fusion of human PCNA (pc2729). For creation of this expression vector, a CMV-driven mRFP-tagged PCNA encoding mammalian expression vector (40) (pc1054) was used to amplify the mRFP-PCNA part with the following primers including restriction sites for XhoI and AflII enzymes (forward**: XhoI** 5'- GCGC**CTCGAG**GA TCTTGGTGGCGTGAAACTC; reverse: **AflII** 5'-GCG CGC**CTTAAG**CCAAACTCACCCTGAAGTTCTC. This amplicon was digested with the corresponding restriction enzymes and ligated to a similarly cut CAG promoter containing mammalian expression vector to generate a mRFP-PCNA fusion gene under the control of the CAG promoter (pc2729). The resulting vector was used to transfect C2C12 and MEF cells. Positive clones were selected using 0.75 μg/ml puromycin (Supplementary Figure S2). Transient transfections of C2C12 and MEF cells were performed using nucleofection (Amaxa NucleoFector II, Lonza Ltd., Basel, Switzerland) with either 1 μg DNA per plasmid (pc1121, pc1467, pc2809, pc1803) or 2 μg per plasmid (pc3086, pc3147, pc2942).

Immunofluorescence

Cells were grown on gelatinized glass coverslips, which were coated for 20 min with 0.2% gelatine from porcine skin (in ddH$_2$O, Sigma-Aldrich, Steinheim, Germany, Cat #: G2500). Cells were fixed in 4% formaldehyde (10 min at room temperature (RT)), permeabilized for 20 min at RT in 0.5% Triton X-100/PBS and unspecific binding sites were blocked with 4% BSA/PBS for 30 min at RT. Immunofluorescence stainings were performed in 4% BSA/PBS for 2 h at RT (primary antibodies) and for 1 h at RT (secondary antibodies). The following primary antibodies were used: rabbit anti-H3K9ac (1/200, Upstate, Lake Placid, USA, Cat #: 06-942), mouse anti-H3K27me3 (1/100, Active Motif, Carlsbad, USA, Cat #: 39535), rabbit anti-H3K27me3 (1/200, Active Motif, Carlsbad, USA, Cat #: 39155), rabbit anti-H3K9me2 (1/200, Biomol, Hamburg, Germany, Cat #: 07-212), mouse anti-H3K9me3 (1/200, Active Motif, Carlsbad, USA, Cat #: 39285), rabbit anti-H3K9me3 (1/200, Upstate, Lake Placid, USA, Cat #: 07-442), rabbit anti-H4K20me3 (1/500, Abcam, Cambridge, UK, Cat

#: ab9053), rabbit anti-Lamin A/C (1/200, kind gift of Ricardo Bastos, Institute Jacques Monod, Paris, France), mouse anti-Lamin B (undiluted, Progen Biotechnik GmbH Heidelberg, Germany, Cat #: 65147C) and mouse anti-Nup153 (1/200, Abcam, Cambridge, UK, Cat #: ab24700). For Lamin B staining, samples were fixed 10 min at RT with ice-cold methanol and were dehydrated prior to standard protocol. The following secondary antibodies were used: donkey-anti-mouse IgG-Cy3 and donkey-anti-rabbit IgG-Cy3 (1/200, Jackson Immuno Research, Baltimore, USA, Cat #: 715-166-151/ 711-165-152). Nuclear DNA was visualized by 4,6-diamidino-2-phenylindole (DAPI, 1 μg/ml, Sigma-Aldrich, Steinheim, Germany, Cat #: D9542). Cells were mounted in Mowiol 4-88 (Sigma-Aldrich, Steinheim, Germany, Cat #: 81381).

In situ replication labeling

For the visualization of replicating DNA, C2C12 mouse myoblasts were pulse labelled for 30 min with 100 μM 5-bromo-2′-deoxyuridine, BrdU (Sigma-Aldrich, Steinheim, Germany, Cat #: 59-14-3) and/or 10 μM 5′-ethynyl-2′-deoxyuridine, EdU (Invitrogen, Carlsbad, USA, Cat #: C10339). For a pulse-chase-pulse experimental setup a 200 μM thymidine chase (Sigma-Aldrich, Steinheim, Germany, Cat #: T1895) was performed in between both pulses. Incorporated BrdU was detected with a rat anti-BrdU antibody (1/200, AbD Serotec, Oxford, UK, Cat #: OBT0030CX) combined with 10 μg/μl DNaseI (Sigma-Aldrich, Steinheim, Germany, Cat #: D5025) for 1 h at 37°C in 4% BSA/PBS. Cells were then washed with 0.5% BSA/1mM EDTA/PBS + 0.01% Tween to stop DNaseI digestion. EdU was detected using ClickIT chemistry (Invitrogen, Carlsbad, USA, Cat #: C10639) as described in (41) with Alexa Fluor 594 (1/300). DNA was counterstained with 1 μg/ml DAPI (Sigma-Aldrich, Steinheim, Germany, Cat #: D9542) for 10 min at RT and cells were mounted in Mowiol.

Major satellite DNA-FISH

For mouse major Satellite DNA-FISH, DNA probes were generated by PCR using biotinylated nucleotides (forward primer: 5′-GCGAGAAAACTGAAAATCAC, reverse primer: 5′-TCAAGTCGTCAAGTGGATG). Briefly, transfected C2C12 cells grown on gelatinized coverslips for 20 or 49 h post-transfection were washed with PBS and fixed with 4% formaldehyde for 10 min at room temperature. After permeabilization with 0.5% Triton-X100 in PBS for 20 min, cells were treated with 0.1 M HCl (for 15 min at RT). After washing with PBS, cells were again permeabilized for 15 min and incubated for 20 min with 50% formamide/saline sodium citrate (SSC) (Carl Roth, Karlsruhe, Germany, Cat #: P040/3957/3580). For FISH probe precipitation, biotinylated probe was incubated with fish sperm DNA (Sigma-Aldrich, Steinheim, Germany,Cat #:74782), 3 M sodium acetate (Carl Roth, Karlsruhe, Germany, Cat #: 6773) and 100% ice-cold ethanol at –80°C for 50 min. After centrifugation for 45 min at 13000 rpm and 4°C, supernatant was removed and the probe was incubated with ice-cold 70% ethanol. The FISH probe was centrifuged for 30 min, the supernatant discarded and the pellet dried for at least 60 min. The dried pellet was dissolved

in a hybridization solution, containing 50% formamide, $2\times$ SSC, 10% dextran sulfate pH 7 (Applichem, Darmstadt, Germany, Cat #: A4970) and was incubated for 45 min at 37°C shaking at 300 rpm. After denaturation for 8 min at 80°C the probe was immediately cooled on ice and put on the fixed and permeabilized cells. The samples were put in a humidified chamber, incubated for 5 min at 80°C and over night at 37°C. Coverslips were washed for 15 min at 45°C in 50% formamide/SSC followed by 10 min in $2\times$ SSC. After blocking in 1% BSA/$4\times$ SSC for 45 min at RT, probes were detected by streptavidin-Cy5 (1/500, Amersham Biosciences, Piscataway, USA, Cat #: PA45001) for 45 min at RT. Nuclear DNA was visualized with DAPI and cells were mounted in Mowiol as described above.

Light microscopy

Confocal images were obtained using an UltraVIEW VoX spinning disc system (PerkinElmer, Massachusetts, USA) on a Nikon Ti microscope equipped with an oil immersion Plan-Apochromat $\times 60/1.45$ numeric aperture objective lens (pixel size in XY = 112 μm, Z-step 0.3–1 μm). Excitation was done using the following laser lines: 405, 488, 561 and 640 nm. Images were taken with the appropriate filters for the respective dyes: DAPI: emission wavelength (em): 415–475 nm; GFP: em: 505–549 nm; RFP: em: 580–650 nm and Cy5: em: 664–754 nm. Z stacks and montages were created using ImageJ (http://rsb.info.nih.gov/ij/). For live-cell microscopy stable C2C12 and stable MEF cell line expressing RFP-PCNA were transfected and plated on a glass bottom p35 dish and grown under standard conditions for at least 20 h. Time-lapse experiments were carried out in a closed live-cell microscopy chamber (ACU control, Olympus) heated to 37°C, with 5% CO_2 and 60% humidity. Z-stacks were acquired with 20 min intervals with a Hamamatsu C9100-50 EMCCD camera.

Electron microscopy

C2C12 cells grown on gelatinized coverslips were fixed with 4% formaldehyde in Sörensen phosphate buffer at 4°C. After fixation, the cells were washed, dehydrated in ethanol and embedded in LRWhite resin (Electron Microscopy Sciences, Hatfield, USA, Cat #: 14381) that was polymerized by heat. The embedded cells were separated from the coverslips after short treatment with liquid nitrogen and cut parallel to the substrate using a Leica Ultracut ultramicrotome. The ultrathin sections of 60 nm were mounted on Formvar/carbon-coated nickel grids and processed for postembedding immunogold labeling. Briefly, the grids with sections were pretreated with 10% normal goat serum (PAA Laboratories, Pasching, Austria, Cat #: B11-035) in PBS for 10 min and then treated, for 17 h at 4°C, with primary antibodies anti-DNA (Progen Biotechnik, Heidelberg, Germany, Cat #: 61014) or anti-H3K9me3 (Abcam, Cambridge, UK, Cat #: ab8898) diluted in PBS containing 0.05% Tween 20 (Sigma-Aldrich, Prague, Czech Republic, Cat #: P1379) and 1% BSA (Sigma-Aldrich, Prague, Czech Republic, Cat #: A3294). As controls for the specificity of detection, some sections were incubated in the absence of primary antibodies. After washing, followed by a repeated treatment with normal goat serum, the sections were reacted with 12 nm colloidal gold-conjugated secondary antibodies (Jackson ImmunoResearch, West Grove, USA, Cat #: 115-205-075, 111-205-144 and 115-205-068) in PBS at room temperature for 30 min. Finally, all grids were thoroughly rinsed, air-dried and stained with aqueous uranyl acetate (Electron Microscopy Sciences, Hatfield, USA, Cat#: 22400) and lead citrate (Electron Microscopy Sciences, Hatfield, USA, Cat#: 17800). The grids were examined with a Morgagni electron microscope (FEI, Eindhoven, The Netherlands) at 80 kV using a 30–40 μm objective aperture. Ten images were taken with a CCD camera MegaView III from each experimental group.

Image analysis and quantification

The area of each chromocenter was determined from the electron microscopy images manually with a cursor. The following cytometric parameters were recorded with the help of Image J: area (in $μm^2$), perimeter (the length of the outside boundary of the selection), aspect ratio (major axis/minor axis), circularity (a value of 1.0 indicates a perfect circle; as the value approaches 0, it indicates an increasingly elongated shape), roundness ($4 \times$ area/($\pi \times$ major axis^2; the inverse of the aspect ratio), and solidity (area/convex area).

The frequency of DNA replication patterns was quantified from the light microscopy images by visual classification of C2C12 cells into early, mid and late S-phase patterns (described in (3)) followed by calculating the respective percentages. An early S-phase pattern is characterized by DNA replication foci distributed homogenously throughout the nucleus with exclusion of the nucle(ol)ar periphery, whereas a mid S-phase pattern is identifiable by well-organized foci at the nucle(ol)ar periphery. Late S-phase is clearly recognizable due to the appearance of fewer but larger clusters of DNA replication foci, colocalizing with chromocenter.

The onset of DNA replication timing of chromocenters in C2C12 and MEF control and targeted cells was analyzed by the colocalization of DNA replication (RFP-PCNA) and chromocenter signal (Mecp2-GFP) and quantified with the H_{coeff} (42). For the calculation of mean post-translational modifications (PTM) levels at pericentric heterochromatin of control and targeted C2C12 and MEF cells, routines were written in the programming language python (http://code.google.com/p/priithon/).

DNA content analysis

C2C12 cells were imaged using the Operetta High Content imaging system (Perkin Elmer, Massachusetts, USA), equipped with a 40×0.95 numeric aperture air objective. For imaging constant exposure times and appropriate filter sets (DAPI: ex: 360–400 nm; em: 410–480 nm; GFP: ex: 460–490 nm; em: 500–560 nm; RFP: ex: 560–580 nm; em: 590–640 nm) were used. Cell segmentation and quantification of nuclear intensities was performed using Harmony (Perkin Elmer, Massachusetts, USA). Subsequently, cells were manually staged for early, mid or late S-phase based on their PCNA pattern as well as assigned whether the cells showed a targeted pattern.

Based on this classification, the total DNA intensity (DAPI) per cell nucleus was plotted for all cells from each replicate. Based on the histogram of all cells per replicate, the DAPI intensity of each cell was normalized to the corresponding G1 and G2 peaks obtained by density fitting. This allowed pooling of the four replicates. Next, the normalized DAPI intensity per nucleus was classified first into non-targeted and targeted pools and, then, in the corresponding S-phase substages.

RESULTS

Manipulating the nuclear position of constitutive heterochromatin

To study the impact of chromatin position on DNA replication, we developed a system to change the sub-nuclear localization of mouse pericentric heterochromatin. Late replicating chromocenters were juxtaposed next to mid replicating facultative heterochromatin to the nuclear periphery. We chose these regions as they have a well-defined epigenetic landscape and form large supra-chromosomal structures, which can be visualized by DNA staining and are a prominent landmark within the nucleus. Our targeting system consisted of two fusion proteins: a chromocenter recognizer (Supplementary Figure S1A) and either GFP binding protein (GBP) tagged-Lamin B1 or Lamin B1 alone (Figure 2). Mecp2-GFP (31) binds strongly to pericentric heterochromatin due to its high levels of DNA methylation. As a control for possible effects of Mecp2-GFP binding and Lamin B1 over-expression on the replication timing or chromatin constitution of chromocenters, we used cells over-expressing Mecp2-GFP and untagged Lamin B1 (Figure 2A) as reference. In these cells, chromocenters showed their typical round structure and position within the nucleus.

In a targeted state, Lamin B1 fusion protein is incorporated into the nuclear lamina like untagged Lamin B1, while its GBP domain (32,33) causes it to interact with Mecp2-GFP (Figure 2B). This interaction resulted in the recruitment of Mecp2, and concomitantly of the pericentric heterochromatin to which Mecp2 was bound, to the nuclear periphery. Major satellite DNA-FISH confirmed that the GFP signal overlapped with pericentric heterochromatin (Figure 2), demonstrating a successful re-localization of chromocenters to the nuclear periphery. Some cells still exhibited a subpopulation of internal chromocenters. This feature was very useful as an internal control, as it allows us to look at differences between peripheral and internal pericentric heterochromatin within the very same cell. After targeted cells went through mitosis, the chromocenters underwent further rearrangements, resulting in their clustering at the top/bottom of the nucleus and forming a star-like cluster (Figure 2B, lower middle row). This secondary rearrangement allowed us to reliably distinguish between cells undergoing the first and second cell cycle after repositioning of chromocenters. After several days of cultivation, whether cells stayed in the targeting mode with star-shaped cluster or whether they exhibited normally localized chromocenters like in control cells, seemed to depend on the transfection efficiency and amount of GBP-LaminB1, which is diluted over the cell cycles.

As shown by these data, our targeting strategy allowed us to manipulate the sub-nuclear localization of pericentric heterochromatin from the nuclear interior to the nuclear periphery. Next, we moved on to use this novel tool to ask whether these position re-arrangements would affect heterochromatin structure, DNA replication timing and epigenetic composition.

Repositioning constitutive heterochromatin affects solidity, area and circularity of targeted chromocenters

First, we addressed the question whether the ultrastructure of constitutive heterochromatin is affected by the repositioning to the nuclear periphery. For this reason, we performed electron microscopy (EM) of Mecp2 control and targeted cells (Figure 3A). In agreement with the FISH data, the EM images showed that whereas control chromocenters are homogenously distributed throughout the whole nucleus, targeted chromocenters are located next to the nuclear lamina. In fact, even the associated nucleolus was repositioned with the respective chromocenter (Figure 3B, right-hand side).

To analyze their ultrastructure we manually selected chromocenters and evaluated different cytometric parameters: solidity, area, circularity, roundness, perimeter and aspect ratio. We found significant differences in the ratio of solidity, area and circularity of control chromocenters versus targeted chromocenters (Figure 3B and Supplementary Table S1). Thus, targeted chromocenters exhibited changed morphology with a less solid appearance but a more elongated shape, whereas control chromocenters retained their prominent, round structure.

Repositioning constitutive heterochromatin does not affect global organization of lamina and nuclear pores

Having demonstrated that our system is proficient to target constitutive heterochromatin to the nuclear lamina, we wanted to evaluate the effect on general nuclear organization. Several lines of evidence support the idea of a relationship between heterochromatin, lamins and nuclear pore complexes (NPC) (43,44).

First, we addressed the question whether the nuclear lamina is affected by the repositioning. For this reason, we performed immuno-detection with antibodies against Lamin A/C and B (Figure 4A). We did not observe differences in the lamin organization in the first cell cycle, comparing control and targeted cells. Whereas in the second cell cycle, the peripheral lamina was mostly unaffected in both control and targeted cells but a fraction of the LaminB colocalized with the star-shaped constitutive heterochromatin cluster of the second cell cycle. Likely, the over-expression of Lamin B1 is involved in the genesis of the star-shaped cluster in the second cell cycle as the Lamin B1 antibody signal colocalized with the targeted chromocenters.

To test whether NPC distribution was altered, we performed immuno-detection with antibodies against Nup153, which is an essential component for the anchoring of NPCs (Figure 4B and Supplementary Table S1). The data showed no differences between control and targeted cells and no colocalization between NPCs and targeted chromocenters
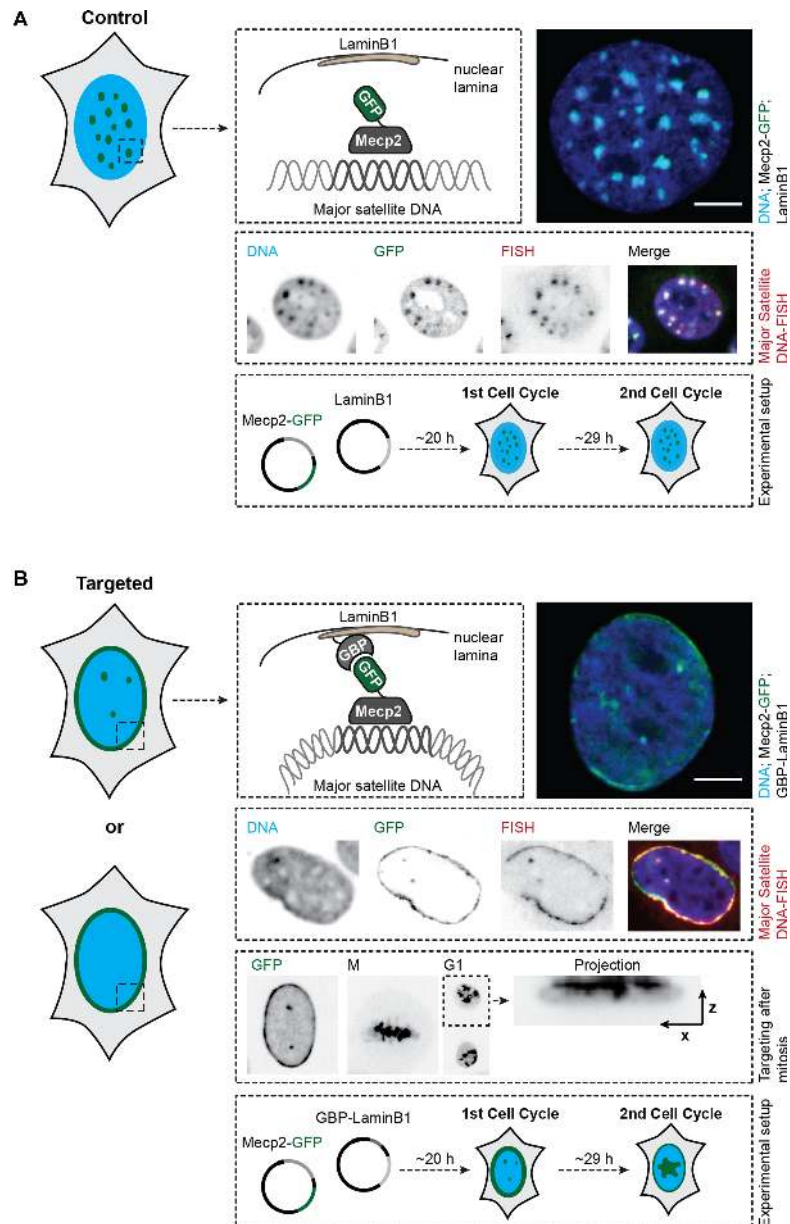
Figure 2. Targeting strategy to reposition chromocenters to the nuclear periphery and its validation by major satellite DNA-FISH. (**A**) In an untargeted state, the fusion protein composed of a chromocenter recognizer Mecp2 and GFP was visible as multiple green fluorescent spots throughout the nucleus, corresponding to constitutive heterochromatin (top section) and colocalized with DAPI dense structures. Untagged Lamin B1, a key component of the nuclear lamina, did not interact with Mecp2-GFP leading to original localized chromocenters throughout the whole nucleus. Mid section of fixed nuclei of an untargeted cell is shown: DAPI stained DNA in blue, Mecp2-GFP in green and untagged Lamin B1. The efficiency of this targeting approach was validated by major Satellite DNA-FISH (middle row), demonstrating a strong colocalization of the green targeting signal and the major satellite DNA-FISH signal: DAPI stained DNA in blue, Mecp2-GFP in green, major satellite DNA-FISH in red and the overlay of all channels (merge). The experimental setup (bottom row) implied the transient transfection of two plasmids: Mecp2-GFP and Lamin B1 followed by an incubation time of either 20 h for first cell cycle studies or 49 h for second cell cycle studies. Scale bar = 5 μm. (**B**) Schematic representation of the targeting approach in a C2C12 targeted cell (bottom section). Upon co-expression of Mecp2-GFP and Lamin-tagged GFP-binding protein (GBP), tagged chromocenters were repositioned to the nuclear periphery (top row). GBP, a *camelidae*-derived nanobody, acts as the key component of the targeting strategy. Because of the strong interaction of GFP and GBP with a Kd in the subnanomolar range, chromocenters were repositioned to the nuclear periphery, clearly visible as a green targeting ring with or without internal chromocenters (two phenotypes possible). The functionality of the targeting was validated by major satellite DNA-FISH (upper middle row), resulting in a strong colocalization of the green targeted chromocenter signal and the major satellite DNA-FISH signal: DAPI stained DNA in blue, Mecp2-GFP and GBP-Lamin B1 in green, major satellite DNA-FISH in red and the overlay of all channels (merge). The efficiency and nontoxicity of this targeting approach was demonstrated by the fact that targeted C2C12 cells were able to undergo mitosis and replicated in a second cell cycle and even further cell cycles (lower middle row). After mitosis the green targeting ring signal no longer appeared as a targeting ring but rather as a 'star'-shaped topologically associated chromocenter cluster. For a better spatial visualization of the star-shaped cluster as a bulk of DNA distributing from the periphery into the inside of the nucleus, a xz projection of the GFP signal is shown. The xz-projection of targeted chromocenters of the second cell cycle showed indeed that these topologically associated chromocenters were still repositioned and localized at the nuclear periphery. The experimental setup (bottom row) required a transient double transfection of Mecp2-GFP and GBP-Lamin B1 followed by an incubation time of either 20 h for the first cell cycle studies or 49 h for second cell cycle studies. Scale bar = 5 μm.
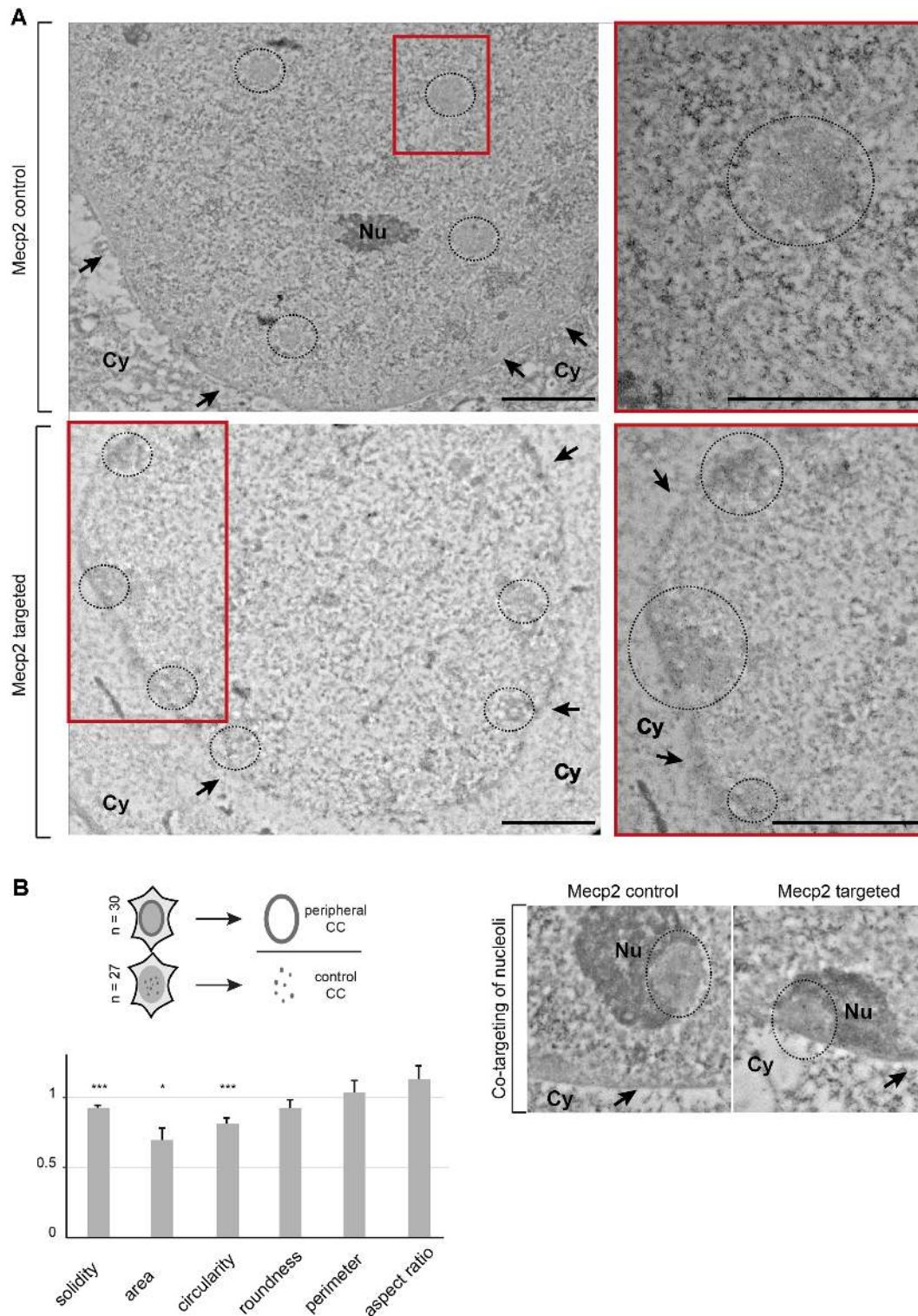
Figure 3. Ultrastructural electron microscopy of repositioned heterochromatin and cytometric analysis. (**A**) Ultrastructural localization of chromocenters in C2C12 control and targeted cells. Top row shows a non-targeted cell labelled with anti-DNA labeling and bottom row depicts a Mecp2 targeted cell. Chromocenters were clearly distinct morphologically and labelled with 12-nm colloidal gold particles upon anti-DNA staining (dashed circles). The micrographs show chromocenters in control cells widely distributed within the nucleoplasm, whereas in targeted cells chromocenters were observed at the nuclear periphery. A region of interest is marked with a red box in the left column (scale bar: 2 μm) and is shown in the right column (scale bar: 1 μm). Arrows depict the nuclear membrane. Cy = cytoplasm; Nu = nucleolus; dashed circles: chromocenters. (**B**) Bar graphs depict the ratios of cytometric parameters of targeted chromocenters normalized to control chromocenters. Significant changes were achieved in the cytometric parameters solidity, area and circularity. Error bars represent 95Cl. Sample sizes (*n*) of chromocenters are indicated on the left-hand side. Statistical significance was tested using the *t*-test, comparing control and targeted chromocenters. *$P < 0.05$; ***$P < 0.001$. Moreover, the interaction of Mecp2-GFP and GBP-Lamin B1 was strong enough to reposition even nucleoli associated with chromocenters to the nuclear periphery (arrows) in C2C12 targeted cells (right hand side).
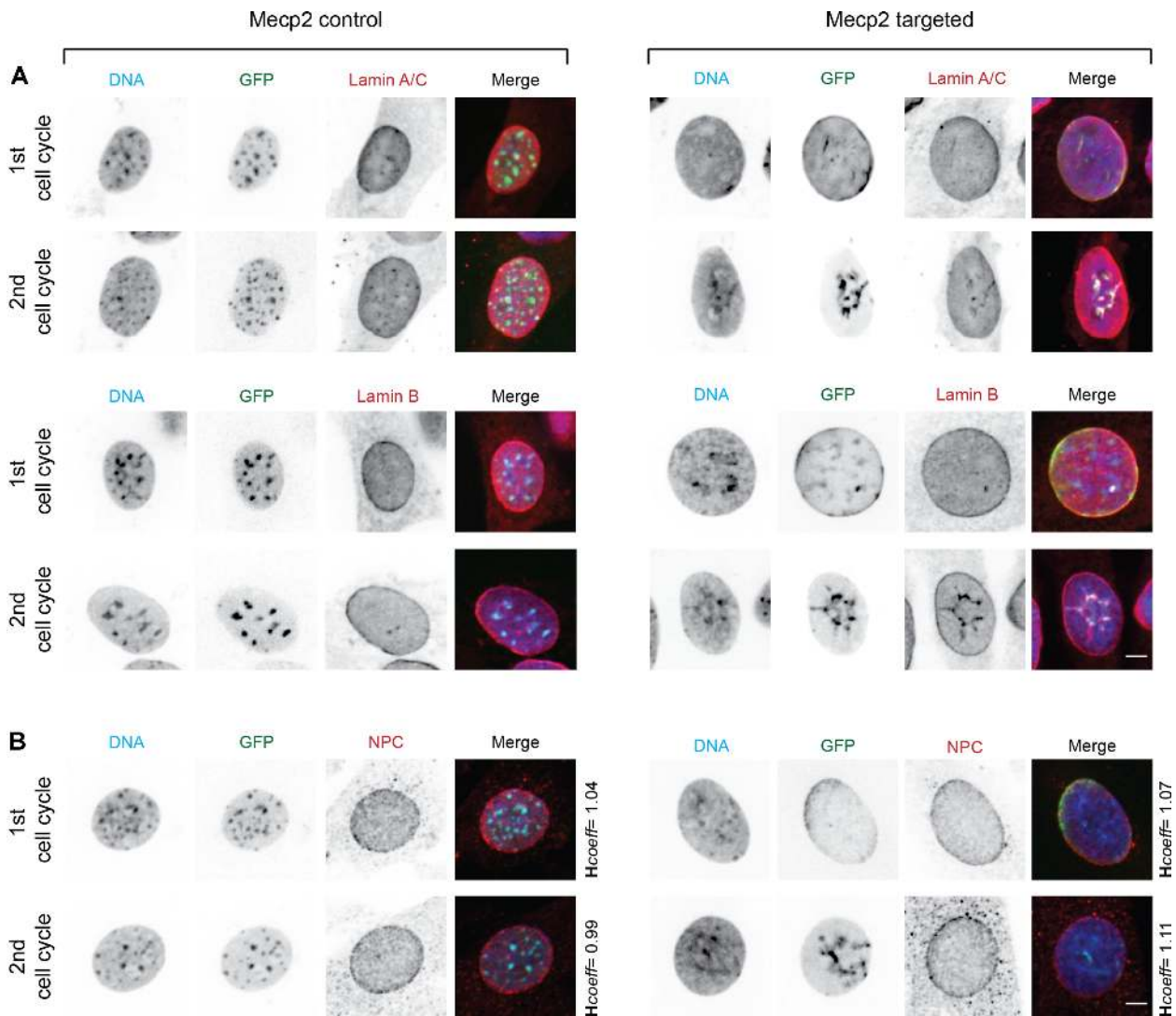
Figure 4. Organization of Lamin A/C, Lamin B and NPCs in control and targeted C2C12 cells. (**A**) C2C12 control and targeted cells were transfected with the appropriate constructs and were either incubated for 20 h for first cell cycle studies or for 49 h for second cell cycle studies. Immunostainings for Lamin A/C and Lamin B were performed. DAPI stained DNA (far left), Mecp2-GFP (mid-left), respective immunostaining (mid right) and merge of all channels (far right). No effect on lamin distribution is detectable, comparing control and targeted C2C12 cells. Only in the second cell cycle, Lamin B1 is colocalizing with the star- shaped chromocenter cluster. Scale bar $= 5$ μm. (**B**) Transfected C2C12 control and targeted cells in the first and the second cell cycle were stained for Nup153. DAPI stained DNA (far left), Mecp2-GFP (mid-left), NPCs (mid right) and merge of all channels (far right). No effect on the NPC distribution is measurable. Values of H_{coeff} colocalization analysis are indicated next to the respective merge. Scale bar $= 5$ μm.

as additionally assayed by measuring the H_{coeff} (42). In this coefficient, particles that exclude each other show an H_{coeff} lower than 1, if particles are randomly distributed with respect to each other, the H_{coeff} is 1 and if they interact, this factor has a value above 1.

As shown by these data, our targeting strategy allowed us to manipulate the sub-nuclear localization of pericentric heterochromatin from the nuclear interior to the periphery without major disruption of the general nuclear organization. Therefore, we used this novel tool to ask whether these position re-arrangements would affect DNA replication timing and/or chromatin composition.

Targeting constitutive heterochromatin to the nuclear periphery increases mid S-phase length

We next asked whether this repositioning would be accompanied by changes in DNA replication timing from late to mid S-phase of the now peripherally located constitutive heterochromatin. If this were the case, we would expect an increase in the percentage of mid S-phase replication patterns due to an increase of mid S-phase duration. To test this hypothesis, we added thymidine analogs for a 30-min pulse to proliferating populations of C2C12 control and targeted cells (Figure 5A). In S-phase cells, which are actively replicating DNA, the thymidine analogs are incorporated into newly synthesized DNA. After detection, S-phase patterns were visually assessed and categorized into early, mid and late S-phase patterns. In con-
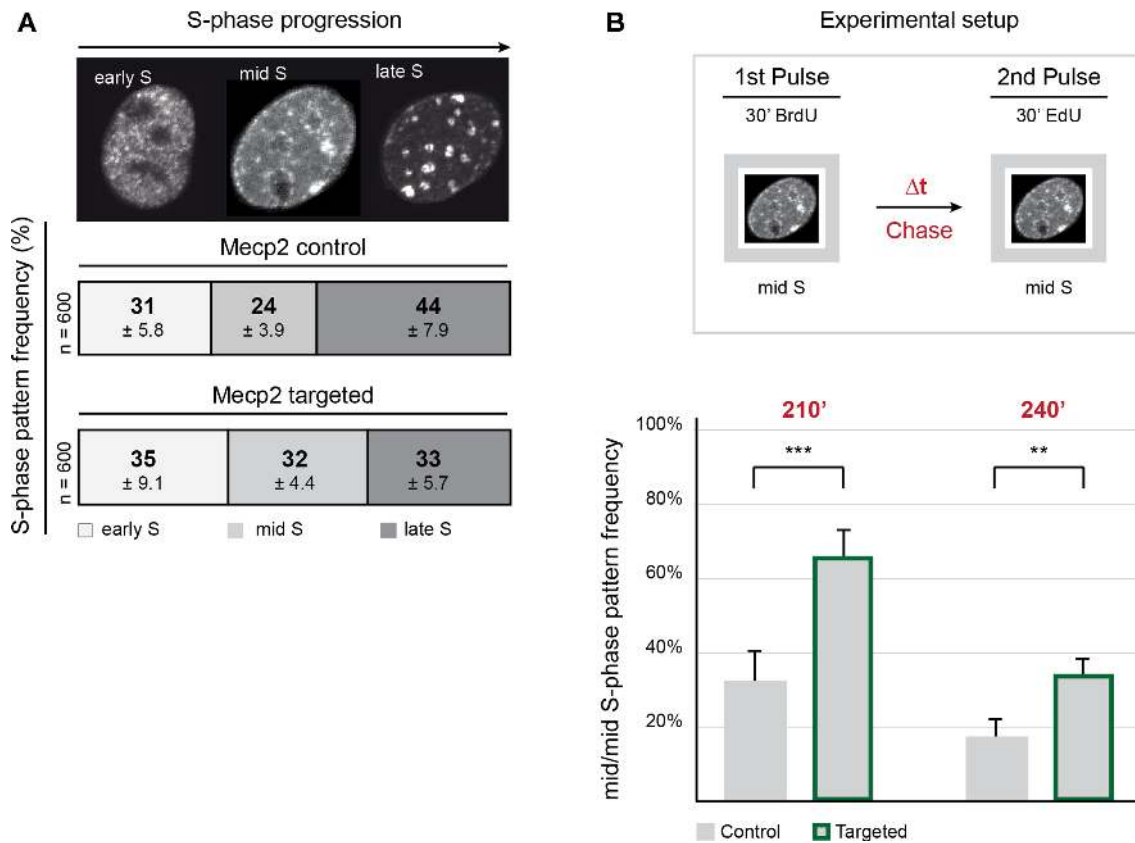
Figure 5. Effect of heterochromatin repositioning on mid S-phase pattern frequency and duration. (**A**) Modified thymidine analogs (BrdU or EdU) were given to the cells for 30 min prior to fixation. Detection thereof and fluorescence microscopy allowed the quantification of early, mid and late DNA replication patterns. Exemplary images of S-phase patterns were depicted to illustrate the categorization into early, mid and late S-phase stages. In C2C12 control cells about 44% of replicating cells showed a late S-phase pattern. In contrast, in targeted cells the frequency of late S-phase replication pattern decreased to 33% with a corresponding increase of mid S-phase replication patterns. Sample sizes are indicated on the left-hand side. Standard deviations of replicates are shown below the numbers in the boxes. (**B**) Schematic representation of the experimental setup to estimate the mid S-duration in C2C12 control and targeted cells. For the quantification, modified thymidine analogues (BrdU and EdU) were added to the culture medium in a pulse-chase-pulse experimental setup. Between 30 min pulses a variable thymidine chase of either 210 or 240 min was performed. Plotted was the percentage of cells that show in the second pulse (EdU) still a mid S-phase pattern (referred as mid/mid). Error bars represent standard deviations of replicates. Statistical significance was tested using the *t*-test, comparing control and targeted C2C12 cells. ***P* < 0.005; ****P* < 0.001.

trol C2C12 cells, about 44% of the S-phase cells exhibited a late S-phase pattern (large labeled structures of constitutive heterochromatin), whereas 24% of cells were identified as mid replicating (perinuclear and perinucleolar foci of facultative heterochromatin). Upon repositioning of constitutive heterochromatin, targeted cells showed a decrease in late S-phase patterns to 33% along with an increase of mid S-phase patterns to 32%.

To test whether the increased frequency of mid S-phase patterns was the result of a prolonged mid S-phase duration, indicating more time required to replicate the extra major satellite DNA repositioned to the nuclear periphery, we set up a replication labeling with two pulses and a variable chase in between (Figure 5B and Supplementary Table S1). Again, thymidine analogs (BrdU and EdU) were added to proliferating populations of C2C12 control and targeted cells prior to fixation in a pulse-chase-pulse experimental protocol. We chose chases of 210 and 240 min as we knew from our S-phase distribution measurements that mid S-phase duration in C2C12 cells lasts ∼3 h and, hence, at least in control cells, we expected complete progression

through mid S-phase during these chase times. We selected all cells that were undergoing mid S-phase during the first pulse (BrdU) and asked whether they stayed in mid S-phase (referred as mid/mid S) or whether they had transitioned into late S-phase after the different chase times. For simplification, we only plotted the percentage of cells that show in both pulses a mid S-phase pattern. Indeed, after a chase of 210 min most control C2C12 cells transitioned from mid S-phase to late S-phase, only a small percentage of cells still persisted in mid S-phase. After a chase of 240 min nearly all untargeted cells exhibited a late S-phase pattern in the second pulse. In contrast, targeted cells did not exhibit this clear decrease of mid S-phase patterns over the same time. After a chase of 210 min there were significantly more cells in mid S-phase (mid/mid S) than in control cells, demonstrating a prolonged duration of mid S-phase patterns detectable in targeted cells. This longer prevalence of mid S-phase patterns suggests that repositioning the normally late replicating constitutive heterochromatin to the nuclear periphery advanced their replication timing to mid S-phase.

Targeting constitutive heterochromatin to the nuclear periphery increases DNA content of targeted cells during mid S-phase

As a next step, we directly measured the amount of genomic DNA synthesized throughout the S-phase of control and targeted cells in C2C12 cells stably expressing RFP-PCNA. We visually categorized replicating cells by PCNA staining pattern in early, mid and late S-phase and in non S-phase cells. We analyzed the integrated DAPI intensity in individual nuclei and normalized all cells of one replicate to the G1 peak intensity (Figure 6A) (for details see (7)). To investigate whether more DNA was replicated during mid S-phase due to repositioning of constitutive heterochromatin to the nuclear periphery, we plotted the relative DNA content (as G1 equivalents) (Figure 6B and Supplementary Table S1). Over time the DNA content increased from G1 towards G2 when cells duplicated their genome. We were able to show that the amount of genomic DNA is significantly increased in mid S-phase in targeted cells. This result is consistent with our previous finding that mid S-phase duration is prolonged in targeted cells, indicating that the repositioned normally late replicating constitutive heterochromatin replicates concomitantly with mid replicating facultative heterochromatin. To test this hypothesis we performed time-lapse microscopy to identify the DNA replication onset of repositioned chromocenters.

Manipulating the sub-nuclear heterochromatin position advances the onset of its DNA replication

To directly analyze the DNA replication onset of repositioned chromocenters, as well as the total duration of S-phase we assessed changes in the timing of peripheral and internal chromocenters in the first and the second cell cycle. For these experiments, we made again use of C2C12 cells stably expressing RFP-PCNA to label active DNA replication sites and co-transfected these cells with Mecp2-GFP to label chromocenters and either Lamin B1 or GBP-Lamin B1. We started the time-lapse imaging either 20 or 49 h post-transfection for analysis of the first and second cell cycle respectively. The combination of fluorescent labels allowed us to measure colocalization of chromocenters (Mecp2-GFP) and DNA replication (RFP-PCNA) signals *in vivo* throughout S-phase. Images were collected every 20 min intervals for up to 16 h, allowing us to unequivocally identify early, mid and late S-phase patterns in the same cell. We used these images to perform three steps of analysis: visual inspection of time-lapse images, line profile intensity measurements and H_{coeff} colocalization analysis (42). We made use of the H_{coeff} to quantify colocalization of signals from chromocenters and DNA replication (Figure 7 and Supplementary Table S1).

Mecp2 control cells (Figure 7A, Video 1) showed clear colocalization of chromocenter and replication signals during late S-phase only. The H_{coeff} analysis confirmed these findings with a value >1 in late S-phase cells. In targeted cells (Figure 7B, Video 2) two regions of interest (ROI) were chosen for the line intensity plot analysis: an untargeted chromocenter (as an internal control) and a peripheral chromocenter. As a consequence of repositioning to the

periphery, we observed colocalization of targeted chromocenters and DNA replication already during mid S-phase, in parallel to facultative heterochromatin (shortly after the inactive X chromosome, Supplementary Figure S3). In contrast, in control or internal chromocenters, we detected very little colocalization between chromocenters and sites of mid S-phase DNA replication. Conversely, these chromocenters showed a strong correlation of both signals in late S-phase. Time-lapse microscopy analysis also showed that the total S-phase length of targeted cells is not significantly affected by the repositioning (Figure 7B).

As Mecp2 is known to recruit other proteins like histone deacetylases, by itself it could have an effect on DNA replication timing. For this reason, we used alternative targeting strategies to exclude that the effects we observed were due to the Mecp2 dependent targeting of chromocenters. To this end, we performed an equivalent set of experiments with DNA sequence-specific chromocenter binders: msTALE, msPZF, msCRISPR/dCas9 (Supplementary Figure S4 and Supplementary Table S2) with a similar outcome, i.e., earlier onset of DNA replication of constitutive heterochromatin. The fact that all four targeting systems to manipulate the position of constitutive heterochromatin resulted in similar effects on DNA replication strengthens our conclusions that the localization of DNA in the nucleus is involved in promoting earlier replication onset of chromocenters.

Next, we addressed the impact of DNA repositioning to the nuclear periphery on the second cell cycle (Figure 7C, Supplementary Figure S5, Video 3). As described above, we observed that after mitosis, upon nuclear envelope reformation, in 100% of the cells the chromocenters adopted a star-shaped cluster at the nuclear periphery of the nucleus. We took advantage of this star-shaped chromocenter cluster to ensure that targeted cells were in the second cell cycle and followed them throughout the following S-phase. The effects on DNA replication timing of repositioned chromocenters in the second cell cycle proved to be even more dramatic than in the first cell cycle. The complete DNA replication of the star-shaped chromocenter cluster took place during mid S-phase, in parallel to the inactive X chromosome (Supplementary Figure S5), as observable in the time-lapse images, by line intensity plot analysis and quantifiable using the H_{coeff}. Mid S-phase was followed by a very short late S-phase with only a few small active DNA replication sites no longer colocalizing with constitutive heterochromatin, also confirmed by the $H_{coeff < }$ 1. The total S-phase duration in the second cell cycle of targeted cells was not dramatically altered (Figure 7B). A slight increase of total S-phase duration in subsequent cell cycles is a known phenomenon due to mild phototoxicity of fluorescent protein imaging over long periods of time. Nevertheless targeted cells in the second cell cycle showed a further increase of mid S-phase duration accompanied with a further decrease of late S-phase duration, shown by time-lapse experiments. To demonstrate that our previous findings are not C2C12 mouse myoblasts specific, we performed the targeting strategy and analysis in addition in mouse embryonic fibroblasts (MEFs), which resulted in the same outcome of earlier DNA replication onset of peripheral constitutive heterochromatin (Supplementary Figure S6 and Supplementary Table S2).
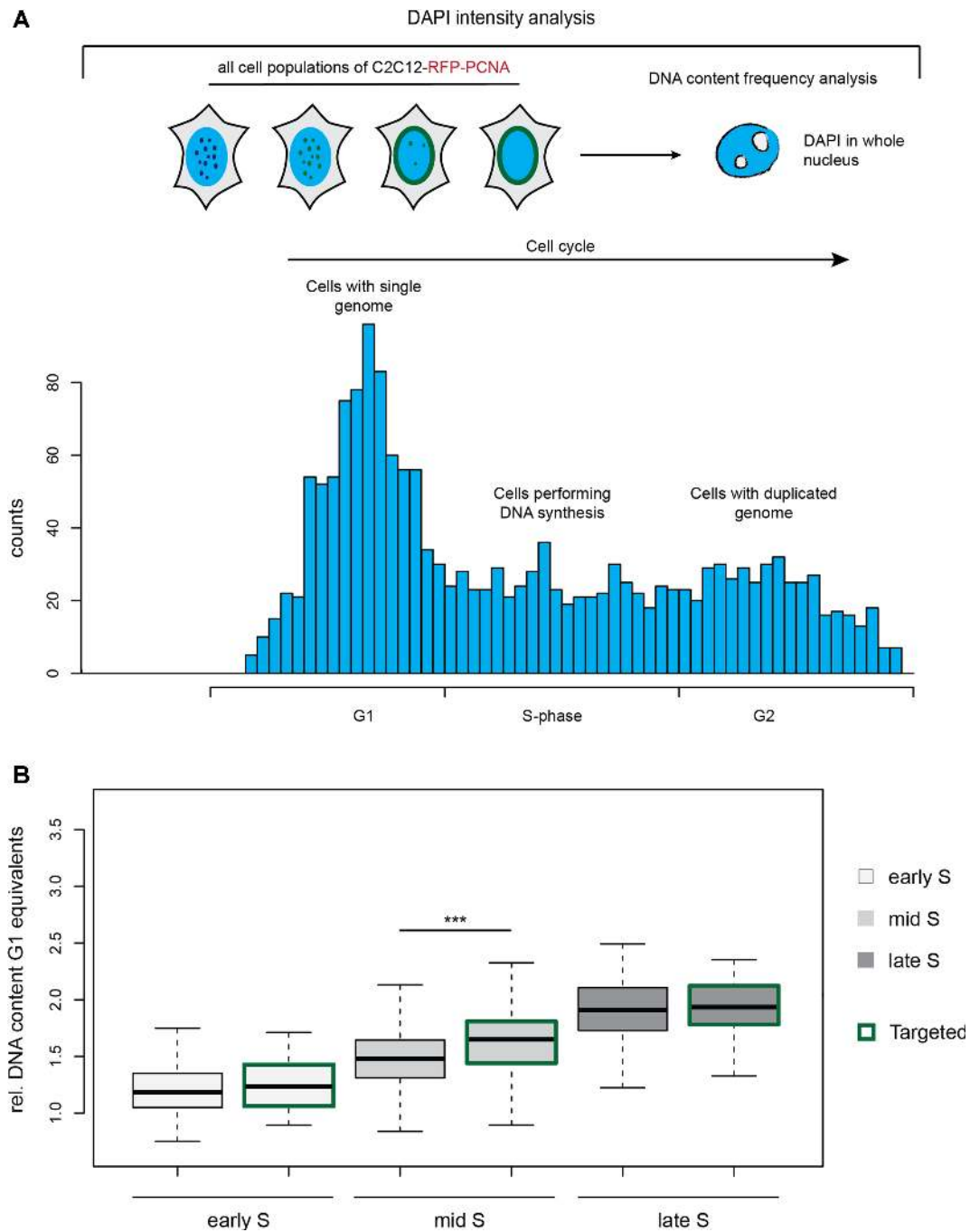
Figure 6. Increase of DNA content in mid S-phase in targeted relative to control cells. (**A**) DNA content frequency analysis throughout the cell cycle. Cells from each replicate ($n > 1000$) are binned by the integrated DNA content (DAPI signal) with the x-axis showing the DNA content of bins in arbitrary units. The first peak represents G1 cells exhibiting a single genome, whereas the second peak corresponds to cells in G2 phase with a duplicated genome. The ratio between the two peak maxima was measured to be 1.93. S-phase cells were manually scored into early, mid and late S-phase. (**B**) Cells from four replicates were normalized to the corresponding G1 peak (set to DNA content of 1) as described in the methods. Box plots depict S-phase substages from early to late for both control and targeted cells. The DNA content of targeted cells in mid S-phase is significantly increased in comparison to non-targeted cells. Statistical significance was tested using the Wilcoxon test, comparing control and targeted C2C12 cells. ***$P < 0.001$.
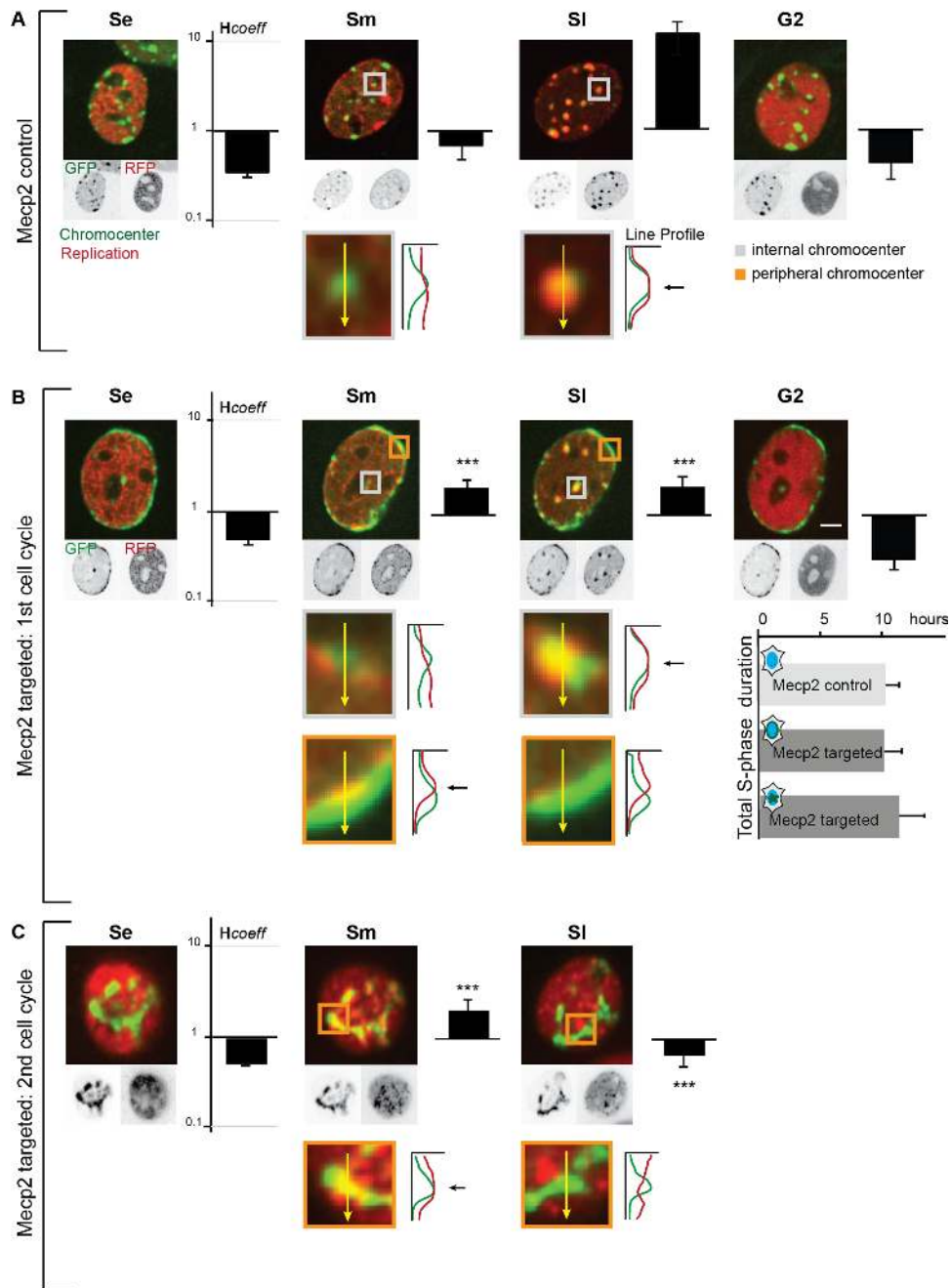
Figure 7. Advanced DNA replication onset in first and second cell cycles in targeted cells, but no effect on total S-phase duration. C2C12 cells stably expressing RFP-PCNA were transfected with Mecp2-GFP and either Lamin B1 (= control) or GBP-Lamin B1 (= targeted) and were incubated for 20 h (**A**, **B**) or 49 h (**C**) and subjected to live-cell time lapse microscopy. (**A**) Representative images depict the different DNA replication patterns in a C2C12 control cell over time. Line intensity plots of DNA replication (red) and chromocenters (green) with a selected ROI of control chromocenter in mid and late S-phase were shown. Control chromocenters showed an increased anti-correlation of DNA replication in mid S-phase, this changed in late S-phase towards high colocalization demonstrating the underlying DNA replication timing of control chromocenters. Colocalization of DNA replication foci and chromocenters was quantified with the H$_{coeff}$ and plotted with bar graphs. H$_{coeff}$ value >1 demonstrated the colocalization of DNA replication foci and control chromocenters in late S-phase. (**B**) Targeted peripheral chromocenters (orange ROI) showed an increased correlation of DNA replication (red) and chromocenters (green) already during mid S-phase, while internal chromocenters (grey ROI) still exhibited an anti-correlation. However, DNA replication of internal chromocenters in a targeted cell took place according to control chromocenters in late S-phase. Scale bar = 5 μm. Increased correlation of DNA replication and targeted chromocenters was verified by an H$_{coeff}$ > 1 already in mid S-phase and only a mild increase was observed in late S-phase of internal chromocenters, whereas there was no correlation at all in early S-phase and G2 cells. Analysis of total S-phase duration from time lapse experiments of Mecp2 control and targeted cells revealed no significant differences in the first and second cell cycles. Error bars represent standard deviations of replicates. Statistical significance was tested using the Wilcoxon test, comparing control and targeted C2C12 cells in the first cell cycle. ***P < 0.001. (**C**) DNA replication timing of targeted C2C12 cells in the second cell cycle. The star-shaped chromocenter cluster started DNA replication during mid S-phase and also completed its DNA replication during mid S-phase. There was only colocalization between DNA replication and chromocenters during mid, whereas there was anti-correlation during late S-phase when only some small foci excluded from chromocenters were replicated. Error bars represent 95 Cl. Statistical significance was tested using the Wilcoxon test, comparing control and targeted C2C12 in the second cell cycle. ***P < 0.001.

In summary, our *in vivo* data demonstrated that, when repositioned to the nuclear periphery, constitutive heterochromatin shifted its replication timing towards mid S-phase and is replicated concomitantly to facultative heterochromatin. These changes in replication timing might be mediated by, result in or be independent of any changes in the composition of pericentric heterochromatin, as defined by post-translational histone modifications. Hence, we next investigated the chromatin marks of the repositioned constitutive heterochromatin.

Histone methylation marks are progressively lost at repositioned constitutive heterochromatin

The nuclear periphery is a region normally occupied by mid S-phase replicating, facultative heterochromatin. Therefore, peripheral targeting of pericentric heterochromatin could potentially change its epigenetic composition to mimic that of facultative heterochromatin. Such changes could in turn be responsible for the earlier onset of DNA replication. We hypothesized three different scenarios: 1) repositioning of chromocenters to the nuclear periphery causes epigenetic changes, which in turn advance DNA replication onset; 2) after replicating out-of-schedule, pericentric heterochromatin changes its typical epigenetic landscape; 3) nuclear position and DNA replication timing change without affecting the epigenetic composition of chromocenters. To test these different hypotheses, we analyzed the effect of peripheral repositioning on the levels of DNA condensation and different histone modifications during the first and second cell cycle.

First, we assessed the condensation level of peripheral chromocenters by analyzing the DNA (DAPI) signal at peripheral versus internal chromocenters in C2C12 cells. We were able to detect a significant decondensation of DNA at peripheral chromocenters in comparison to the internal ones (Figure 8A and Supplementary Table S1).

Next, we tested the effect of nuclear localization on the epigenetic composition of pericentric heterochromatin. To this end, we measured the levels of its characteristic chromatin marks by immuno-detection of various post-translational modifications (PTMs). This allowed us to quantify any changes in the levels of the respective epigenetic modification within chromocenters. The modifications investigated included H3K9 acetylation (H3K9ac), H3K27 trimethylation (H3K27me3), H3K9 dimethylation (H3K9me2), H3K9 trimethylation (H3K9me3) and H4K20 trimethylation (H4K20me3) (Figure 8B, Supplementary Figures S7, S8 and Supplementary Table S1). For this purpose, we developed a user-independent routine measuring the mean PTM levels at pericentric chromatin (for details see Supplementary Figure S9). We made use of the internal chromocenters of partially targeted cells as control to quantify potential differences in the levels of PTMs for the first cell cycle and control cell chromocenters for the second cell cycle measurements.

H3K9ac, a mark of transcriptionally active chromatin, was enriched in euchromatic regions. In both, control and targeted cells, this mark was excluded from DAPI dense regions as well as from GFP-labeled chromocenters, corresponding to constitutive heterochromatin regions. Mean

H3K9ac levels showed a mild decrease at peripheral chromocenters in contrast to internal chromocenters (Figure 8B) and this was also the case in MEFs as well as when using sequence specific chromocenter binders (Supplementary Figures S10, S11 and Supplementary Table S2). Thus, we conclude that earlier onset of replication was not caused by increased histone acetylation upon nuclear repositioning.

We then investigated the distribution patterns of four epigenetic marks characteristic of heterochromatin, two enriched at facultative heterochromatic regions, usually found at the nuclear periphery, and two enriched in constitutive heterochromatin. Both H3K27me3 and H3K9me2 as markers for facultative heterochromatin were increased at the nucle(ol)ar periphery as well as, in the case of H3K27me3, on the inactive X chromosome(s) of the female cells. Due to the quasi-tetraploidy of C2C12 cells (23), two inactive X chromosomes were stained in control and targeted cells. However, neither of these modifications colocalized with constitutive heterochromatin, even when it was targeted to the nuclear periphery. The level of H3K27me3 stayed the same in control and targeted cells, whereas the level of H3K9me2 decreased over the second cell cycle in comparison to control cells. Prominent marks for constitutive heterochromatin like H3K9me3 and H4K20me3 showed a strong signal overlapping with DAPI-positive regions and GFP-stained chromocenters in control cells and partially also in targeted cells. Altogether, the level of these constitutive heterochromatin marks decreased over subsequent cell cycles in contrast to the control cells, indicating a progressive loss of the typical histone methylation marks. To rule out any change caused by the targeting strategy via Mecp2 binding or specific to C2C12 cells, we performed these experiments also for targeted cells via sequence-specific targeting (Supplementary Figure S10) as well as with MEF cells (Supplementary Figure S11). Typical constitutive heterochromatin marks were decreased for the sequence-specific binding, whereas in MEF cells H3K9me3 was more stable and only H4K20me3 was lost over time.

DISCUSSION

In this study, we developed strategies to change the position of constitutive heterochromatin within the murine nucleus. Our targeting approach, based on the strong interaction between GFP and GBP, provides a very potent tool, suitable to tether different chromatin regions of interest to specific regions within the nucleus. Our assay, therefore, provides the novel opportunity to study the effect of nuclear position on a variety of genomic processes. By combining this approach with quantitative microscopy, we were able to study nuclear position as a potential regulator of DNA replication timing (Figure 9). We show that repositioning chromocenters to the nuclear periphery and thereby transferring late replicating constitutive heterochromatin into a mid S-phase replicating environment, results in an earlier onset of replication of repositioned chromocenters. This effect was associated with a higher mid S-phase pattern frequency and a longer mid S-phase length. Furthermore, we were able to demonstrate that the DNA content is increased in targeted cells in mid S-phase. This result is consistent with the notion that more time in mid S-phase is required to replicate
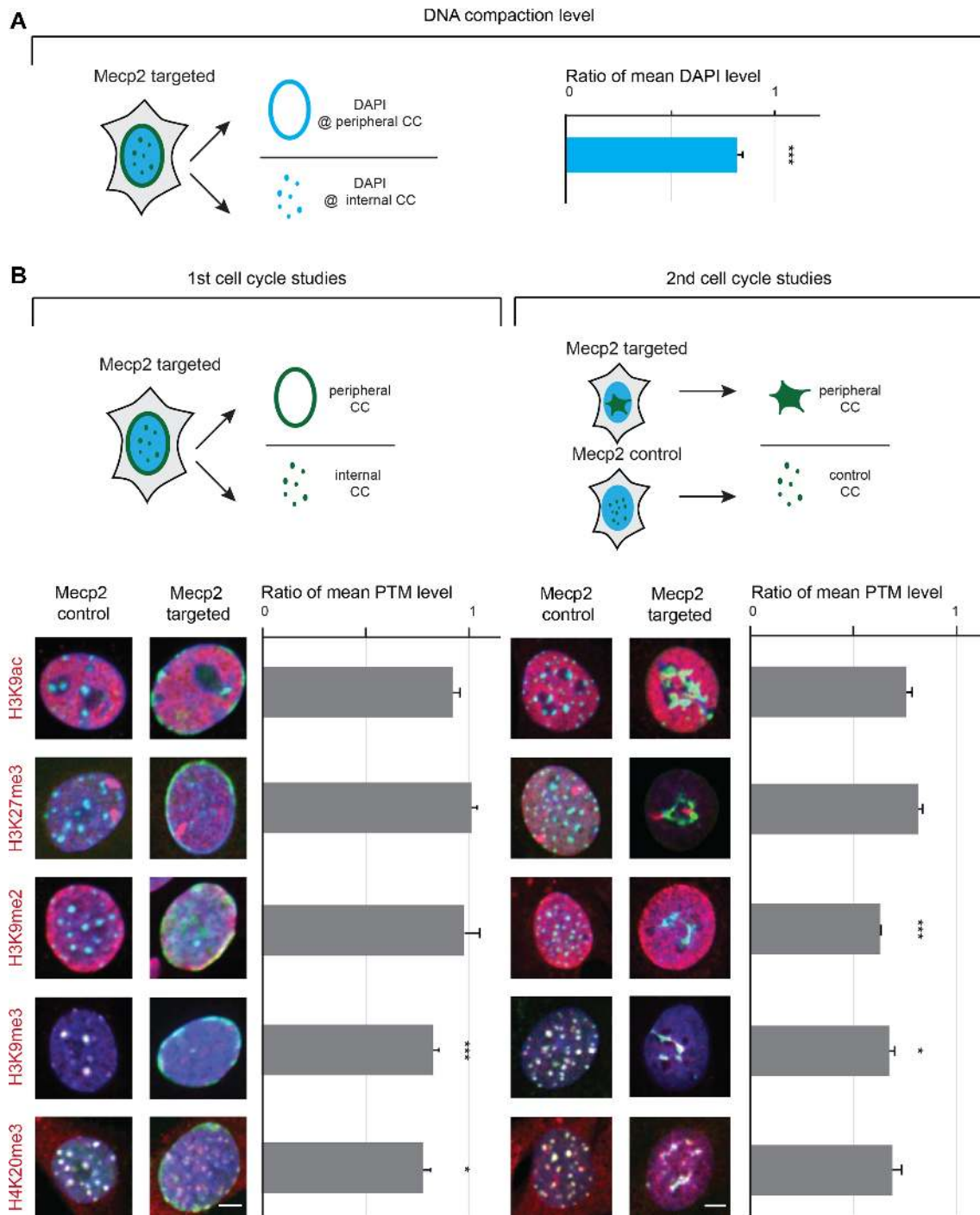
Figure 8. Distribution of prominent chromatin marks in control and targeted C2C12 cells. (**A**) DNA density was measured in Mecp2 targeted cells with the help of a user-independent analysis. The mean DAPI level was measured at peripheral versus internal chromocenters to estimate their compaction level. Bar graphs demonstrate the ratio of mean DAPI levels of peripheral versus internal chromocenters, indicating a significant decrease of condensation level of peripheral ones. Error bars represent 95% Cl. Statistical significance was tested using the Wilcoxon test, comparing peripheral and internal chromocenters. ***$P < 0.001$. (**B**) Prominent chromatin marks were analyzed by immunostainings: H3K9ac (euchromatin), H3K27me3 (facultative heterochromatin), H3K9me2 (marker for chromatin at the nuclear periphery), H3K9me3 and H4K20me3 (constitutive heterochromatin). Top row depicts the rationale of the user-independent analysis and the normalization of mean PTM values. Exemplary images show merges of all channels: DAPI stained DNA (blue), Mecp2-GFP (green), post-translational modification (PTM, red). Scale bar = 5 μm. Bar graphs demonstrate the ratio of mean PTM levels at peripheral versus internal chromocenters. Error bars represent 95% Cl. Statistical significance was tested using the *t*-test, comparing control or internal chromocenters and targeted chromocenters. *$P < 0.05$; ***$P < 0.001$.
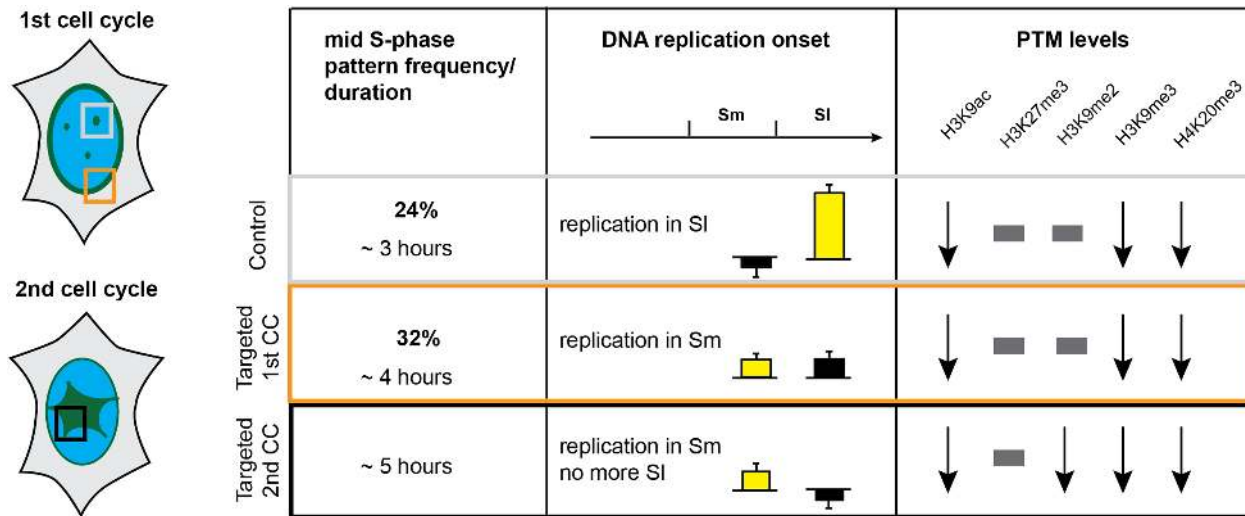
Figure 9. Summary of the effects of DNA position on its replication timing and epigenetic composition. In targeted cells, during the first cell cycle (orange box), the mid S-phase pattern frequency was increased, going hand in hand with a prolongation of mid S-phase duration and this was even more dramatic in the second cell cycle (black box). This was the result of earlier onset of replication of chromocenters that were repositioned in targeted cells to the nuclear periphery. The peripheral chromocenters were replicated already during mid S-phase, whereas, in the same cell, the non-repositioned internal chromocenters were still replicated during late S-phase, indicated by H_{coeff} values over 1 in mid and late S-phase. Changes in the PTM level were indicated with arrows and no changes are illustrated by the grey rectangles. Chromocenters known to be hypoacetylated and enriched in H3K9me3 and H4K20me3, still showed these characteristic marks, only in decreased levels in comparison to control or internal chromocenters. The repositioning affected the reestablishment of the proper levels of the most characteristic histone marks leading to their progressive loss over subsequent cell cycles. The characteristic epigenetic marks for peripheral chromatin were not added *de novo* to the relocated constitutive heterochromatin.

this out-of-schedule DNA at the nuclear periphery. These data suggest that the total number of active origins at any given time remains constant, in accordance to a limiting factor model (reviewed in (45)). The fact that repositioned chromatin adopts the replication timing of the neighboring facultative heterochromatin supports the idea that adjacent active origins of facultative heterochromatin triggered the earlier DNA replication onset of repositioned chromocenters. According to the domino effect model (46), stochastic activation of the first origin clusters leads to a chain reaction of activation of later origin clusters depending on the relative spatial distribution in the genome within the nucleus (Supplementary Figure S12). Hence, we propose that the concentration of (regulatory) replication factors at the nuclear periphery during mid S-phase creates a microenvironment that enhances the firing efficiency/probability of origins in the nearby, repositioned constitutive heterochromatin. Upon targeting two parameters influencing origin firing are likely coming together: a high local concentration of DNA at the periphery as well as a high concentration of replisomes loaded on facultative heterochromatin. This hypothesis would also explain why chromocenters originally located in inner nuclear regions, surrounded by early replicating chromatin, are not generally triggered to fire earlier in S-phase. In an early replicating nucleus, euchromatin is distributed throughout the whole nucleus and, consequently, concentrations of DNA and replisomes are generally low. This is in contrast to the situation when chromocenters are repositioned to the nuclear periphery where facultative heterochromatin is highly concentrated and replisomes are locally enriched in mid S-phase. Thus, we propose that normally late replicating origins of repositioned chromocenters were triggered by mid replicating origins in a domino-like manner, working not only in *cis* along the chromosome fiber, but rather also in *trans* across different chromosomes within the 3D nuclear space. One important consideration is that the effects on DNA replication timing are not targeting method specific (Supplementary Figure S4) or cell line specific (Supplementary Figure S6), generalizing the regulatory role of nuclear position of DNA on its DNA replication timing.

Finally, we tested whether the epigenetic composition of chromocenters was affected by the repositioning to the nuclear periphery and whether this is a cause or a consequence thereof. The peripherally located chromocenters did exhibit a decrease in the normal levels of the histone methylation marks characteristic for constitutive heterochromatin. These marks were progressively lost over subsequent cell cycles. This suggests that the advanced DNA replication that results from the repositioning of chromocenters to the nuclear periphery affects the re-establishment of chromatin modifications after replication. Conversely, the characteristic epigenetic marks of peripheral facultative chromatin were not added *de novo* to the relocated constitutive heterochromatin. Moreover, the low levels of histone acetylation at chromocenters were maintained regardless of their nuclear location. Previous studies have shown that histone hypoacetylation is the main regulator of the late replication timing of chromocenters and neither H3K9me3 nor large-scale chromatin decondensation were directly involved in defining the late replication timing of constitutive heterochromatin (19). The latter strongly suggests that the advanced replication timing we observed is not a result of changes in the chromatin marks on pericentric heterochromatin.

Shang *et al.* (47) set up a repositioning assay in *cis* along the chromosome. They developed a chromosome engineering system in chicken DT40 cells that allowed the efficient excision of the native centromere and the selection of chromosomes with neocentromeres. When a neocentromere was introduced into an early or early/mid replicating domain this resulted in a shift of the surrounding regions, which were previously early replicating, to a later DNA replication timing. When introducing the neocentromere into a late replicating domain, the replication timing of the domain was not altered. This study demonstrated that the insertion of a neocentromere seems to have affected the DNA replication timing of the surrounding domain *in cis*. It is though not clear whether this is due to impact of the neocentromere insertion in the chromatin state of the domain where it was inserted or on transcriptional activity of the domain. It is also unclear whether the 3D spatial nuclear distribution of the domain was altered upon neocentromere insertion. Whereas in Shang *et al.* (47) the receiving chromatin domain adopts the replication timing of the inserted neocentromere, in our study, positioning of constitutive heterochromatin in a facultative heterochromatin environment *in trans*, affected rather the replication timing of the repositioned chromatin.

Taken together, we propose that the nuclear position directly affects DNA replication timing of peripheral chromocenters, independently of changes in histone modifications. Furthermore, the changed position and replication timing of constitutive heterochromatin impairs post-replicative establishment of chromatin marks.

SUPPLEMENTARY DATA

Supplementary Data are available at NAR Online.

REFERENCES

1. Chagin,V.O., Stear,J.H. and Cardoso,M.C. (2010) Organization of DNA replication. *Cold Spring Harb. Perspect. Biol.*, **2**, a000737.
2. Jackson,D.A. and Pombo,A. (1998) Replicon clusters are stable units of chromosome structure: evidence that nuclear organization contributes to the efficient activation and propagation of S phase in human cells. *J. Cell Biol.*, **140**, 1285–1295.
3. Leonhardt,H., Rahn,H.P., Weinzierl,P., Sporbert,A., Cremer,T., Zink,D. and Cardoso,M.C. (2000) Dynamics of DNA replication factories in living cells. *J. Cell Biol.*, **149**, 271–280.
4. Nakamura,H., Morita,T. and Sato,C. (1986) Structural organizations of replicon domains during DNA synthetic phase in the mammalian nucleus. *Exp. Cell Res.*, **165**, 291–297.
5. Fox,M.H., Arndt-Jovin,D.J., Jovin,T.M., Baumann,P.H. and Robert-Nicoud,M. (1991) Spatial and temporal distribution of DNA replication sites localized by immunofluorescence and confocal microscopy in mouse fibroblasts. *J. Cell Sci.*, **99**, 247–253.
6. Baddeley,D., Chagin,V.O., Schermelleh,L., Martin,S., Pombo,A., Carlton,P.M., Gahl,A., Domaing,P., Birk,U., Leonhardt,H. *et al.* (2010) Measurement of replication structures at the nanometer scale using super-resolution light microscopy. *Nucleic Acids Res.*, **38**, e8.
7. Lob,D., Lengert,N., Chagin,V.O., Reinhart,M., Casas-Delucchi,C.S., Cardoso,M.C. and Drossel,B. (2016) 3D replicon distributions arise from stochastic initiation and domino-like DNA replication progression. *Nat. Commun.*, **7**, 11207.
8. Chagin,V.O., Casas-Delucchi,C.S., Reinhart,M., Schermelleh,L., Markaki,Y., Maiser,A., Bolius,J.J., Bensimon,A., Fillies,M., Domaing,P. *et al.* (2016) 4D Visualization of replication foci in mammalian cells corresponding to individual replicons. *Nat. Commun.*, **7**, 11231.
9. Casas-Delucchi,C.S. and Cardoso,M.C. (2011) Epigenetic control of DNA replication dynamics in mammals. *Nucleus*, **2**, 370–382.
10. Pope,B.D. and Gilbert,D.M. (2013) The replication domain model: regulating replicon firing in the context of large-scale chromosome architecture. *J. Mol. Biol.*, **425**, 4690–4695.
11. Farkash-Amar,S., Lipson,D., Polten,A., Goren,A., Helmstetter,C., Yakhini,Z. and Simon,I. (2008) Global organization of replication time zones of the mouse genome. *Genome Res.*, **18**, 1562–1570.
12. Hyrien,O. (2015) Peaks cloaked in the mist: the landscape of mammalian replication origins. *J. Cell Biol.*, **208**, 147–160.
13. Gilbert,D.M. (2001) Making sense of eukaryotic DNA replication origins. *Science*, **294**, 96–100.
14. Cayrou,C., Coulombe,P., Puy,A., Rialle,S., Kaplan,N., Segal,E. and Mechali,M. (2012) New insights into replication origin characteristics in metazoans. *Cell Cycle*, **11**, 658–667.
15. Cayrou,C., Coulombe,P., Vigneron,A., Stanojcic,S., Ganier,O., Peiffer,I., Rivals,E., Puy,A., Laurent-Chabalier,S., Desprat,R. *et al.* (2011) Genome-scale analysis of metazoan replication origins reveals their organization in specific but flexible sites defined by conserved features. *Genome Res.*, **21**, 1438–1449.
16. Raghuraman,M.K., Brewer,B.J. and Fangman,W.L. (1997) Cell cycle-dependent establishment of a late replication program. *Science*, **276**, 806–809.
17. Aladjem,M.I. (2007) Replication in context: dynamic regulation of DNA replication patterns in metazoans. *Nat. Rev. Genet.*, **8**, 588–600.
18. Schwaiger,M., Stadler,M.B., Bell,O., Kohler,H., Oakeley,E.J. and Schubeler,D. (2009) Chromatin state marks cell-type- and gender-specific replication of the Drosophila genome. *Genes Dev.*, **23**, 589–601.
19. Casas-Delucchi,C.S., van Bemmel,J.G., Haase,S., Herce,H.D., Nowak,D., Meilinger,D., Stear,J.H., Leonhardt,H. and Cardoso,M.C. (2012) Histone hypoacetylation is required to maintain late replication timing of constitutive heterochromatin. *Nucleic Acids Res.*, **40**, 159–169.
20. Jorgensen,H.F., Azuara,V., Amoils,S., Spivakov,M., Terry,A., Nesterova,T., Cobb,B.S., Ramsahoye,B., Merkenschlager,M. and Fisher,A.G. (2007) The impact of chromatin modifiers on the timing of locus replication in mouse embryonic stem cells. *Genome Biol.*, **8**, R169.
21. O'Keefe,R.T., Henderson,S.C. and Spector,D.L. (1992) Dynamic organization of DNA replication in mammalian cell nuclei: spatially and temporally defined replication of chromosome-specific alpha-satellite DNA sequences. *J. Cell Biol.*, **116**, 1095–1110.
22. Wu,R., Singh,P.B. and Gilbert,D.M. (2006) Uncoupling global and fine-tuning replication timing determinants for mouse pericentric heterochromatin. *J. Cell Biol.*, **174**, 185–194.
23. Casas-Delucchi,C.S., Brero,A., Rahn,H.P., Solovei,I., Wutz,A., Cremer,T., Leonhardt,H. and Cardoso,M.C. (2011) Histone acetylation controls the inactive X chromosome replication dynamics. *Nat. Commun.*, **2**, 222.

24. Kemp,M.G., Ghosh,M., Liu,G. and Leffak,M. (2005) The histone deacetylase inhibitor trichostatin A alters the pattern of DNA replication origin activity in human cells. *Nucleic Acids Res.*, **33**, 325–336.
25. Schwaiger,M., Kohler,H., Oakeley,E.J., Stadler,M.B. and Schubeler,D. (2010) Heterochromatin protein 1 (HP1) modulates replication timing of the Drosophila genome. *Genome Res.*, **20**, 771–780.
26. Vogelauer,M., Rubbi,L., Lucas,I., Brewer,B.J. and Grunstein,M. (2002) Histone acetylation regulates the time of replication origin firing. *Mol. Cell*, **10**, 1223–1233.
27. Dimitrova,D.S. and Gilbert,D.M. (1999) The spatial position and replication timing of chromosomal domains are both established in early G1 phase. *Mol. Cell*, **4**, 983–993.
28. Ebrahimi,H., Robertson,E.D., Taddei,A., Gasser,S.M., Donaldson,A.D. and Hiraga,S. (2010) Early initiation of a replication origin tethered at the nuclear periphery. *J. Cell Sci.*, **123**, 1015–1019.
29. Jones,K.W. (1970) Chromosomal and nuclear location of mouse satellite DNA in individual cells. *Nature*, **225**, 912–915.
30. Vissel,B. and Choo,K.H. (1989) Mouse major (gamma) satellite DNA is highly conserved and organized into extremely long tandem arrays: implications for recombination between nonhomologous chromosomes. *Genomics*, **5**, 407–414.
31. Brero,A., Easwaran,H.P., Nowak,D., Grunewald,I., Cremer,T., Leonhardt,H. and Cardoso,M.C. (2005) Methyl CpG-binding proteins induce large-scale chromatin reorganization during terminal differentiation. *J. Cell Biol.*, **169**, 733–743.
32. Rothbauer,U., Zolghadr,K., Muyldermans,S., Schepers,A., Cardoso,M.C. and Leonhardt,H. (2008) A versatile nanotrap for biochemical and functional studies with fluorescent fusion proteins. *Mol. Cell. Proteomics*, **7**, 282–289.
33. Rothbauer,U., Zolghadr,K., Tillib,S., Nowak,D., Schermelleh,L., Gahl,A., Backmann,N., Conrath,K., Muyldermans,S., Cardoso,M.C. *et al.* (2006) Targeting and tracing antigens in live cells with fluorescent nanobodies. *Nat. Methods*, **3**, 887–889.
34. Kirchhofer,A., Helma,J., Schmidthals,K., Frauer,C., Cui,S., Karcher,A., Pellis,M., Muyldermans,S., Casas-Delucchi,C.S., Cardoso,M.C. *et al.* (2010) Modulation of protein properties in living cells using nanobodies. *Nat. Struct. Mol. Biol.*, **17**, 133–138.
35. Thanisch,K., Schneider,K., Morbitzer,R., Solovei,I., Lahaye,T., Bultmann,S. and Leonhardt,H. (2014) Targeting and tracing of specific DNA sequences with dTALEs in living cells. *Nucleic Acids Res.*, **42**, e38.
36. Lindhout,B.I., Fransz,P., Tessadori,F., Meckel,T., Hooykaas,P.J. and van der Zaal,B.J. (2007) Live cell imaging of repetitive DNA sequences via GFP-tagged polydactyl zinc finger proteins. *Nucleic Acids Res.*, **35**, e107.
37. Anton,T., Bultmann,S., Leonhardt,H. and Markaki,Y. (2014) Visualization of specific DNA sequences in living mouse embryonic stem cells with a programmable fluorescent CRISPR/Cas system. *Nucleus*, **5**, 163–172.
38. Yaffe,D. and Saxel,O. (1977) Serial passaging and differentiation of myogenic cells isolated from dystrophic mouse muscle. *Nature*, **270**, 725–727.
39. Peters,A.H., O'Carroll,D., Scherthan,H., Mechtler,K., Sauer,S., Schofer,C., Weipoltshammer,K., Pagani,M., Lachner,M., Kohlmaier,A. *et al.* (2001) Loss of the Suv39h histone methyltransferases impairs mammalian heterochromatin and genome stability. *Cell*, **107**, 323–337.
40. Sporbert,A., Domaing,P., Leonhardt,H. and Cardoso,M.C. (2005) PCNA acts as a stationary loading platform for transiently interacting Okazaki fragment maturation proteins. *Nucleic Acids Res.*, **33**, 3521–3528.
41. Salic,A. and Mitchison,T.J. (2008) A chemical method for fast and sensitive detection of DNA synthesis in vivo. *Proc. Natl. Acad. Sci. U.S.A.*, **105**, 2415–2420.
42. Herce,H.D., Casas-Delucchi,C.S. and Cardoso,M.C. (2013) New image colocalization coefficient for fluorescence microscopy to quantify (bio-)molecular interactions. *J. Microsc.*, **249**, 184–194.
43. Maeshima,K., Yahata,K., Sasaki,Y., Nakatomi,R., Tachibana,T., Hashikawa,T., Imamoto,F. and Imamoto,N. (2006) Cell-cycle-dependent dynamics of nuclear pores: pore-free islands and lamins. *J. Cell Sci.*, **119**, 4442–4451.
44. Shimi,T., Pfleghaar,K., Kojima,S., Pack,C.G., Solovei,I., Goldman,A.E., Adam,S.A., Shumaker,D.K., Kinjo,M., Cremer,T. *et al.* (2008) The A- and B-type nuclear lamin networks: microdomains involved in chromatin organization and transcription. *Genes Dev.*, **22**, 3409–3421.
45. Rhind,N. and Gilbert,D.M. (2013) DNA replication timing. *Cold Spring Harb. Perspect. Biol.*, **5**, a010132.
46. Sporbert,A., Gahl,A., Ankerhold,R., Leonhardt,H. and Cardoso,M.C. (2002) DNA polymerase clamp shows little turnover at established replication sites but sequential de novo assembly at adjacent origin clusters. *Mol. Cell*, **10**, 1355–1365.
47. Shang,W.H., Hori,T., Martins,N.M.C., Toyoda,A., Misu,S., Monma,N., Hiratani,I., Maeshima,K., Ikeo,K., Fujiyama,A. *et al.* (2013) Chromosome engineering allows the efficient isolation of vertebrate neocentromeres. *Dev. Cell*, **24**, 635–648.